Pure appl. geophys. 165 (2008) 567–583
0033–4553/08/030567–17
DOI 10.1007/s00024-008-0321-0

Pure and Applied Geophysics

3-D Simulation of Steady Plate Subduction with Tectonic Erosion: Current Crustal Uplift and Free-Air Gravity Anomaly in Northeast Japan

CHIHIRO HASHIMOTO,[1] TOSHINORI SATO,[2] and MITSUHIRO MATSU'URA[1]

Abstract—Free-air gravity anomaly in plate subduction zones, characterized by island-arc high, trench low and outer-rise gentle high, reflects the cumulative effects of long-term crustal uplift and subsidence. In northeast Japan the island-arc high of observed free-air gravity anomaly takes its maximum about the eastern coastline. On the other hand, the current vertical crustal motion estimated from geological and geomorphological observations shows a gentle uplift in the land area and steep subsidence in the sea area with the neutral point near the eastern coastline. Such a discrepancy in spatial patterns between the free-air gravity anomaly and current vertical crustal motion can be ascribed to a change in the mode of crustal uplift and subsidence associated with the initiation of tectonic erosion at the North American-Pacific plate interface. We developed a realistic 3-D simulation model of steady plate subduction with tectonic erosion in northeast Japan on the basis of elastic/viscoelastic dislocation theory. Through numerical simulations with this model we found that simple steady plate subduction brings about the crustal uplift characterized by island-arc high with its maximum about the eastern coastline, while steady plate subduction with tectonic erosion, which is represented by the landward retreat of the plate interface, brings about gentle uplift in the land area and steep subsidence in the sea area with the neutral point near the eastern coastline. Therefore, if we suppose that tectonic erosion started 3–4 million years ago after the long duration of simple steady plate subduction, we can consistently explain both patterns of free-air gravity anomaly and current crustal uplift in northeast Japan.

Key words: Plate subduction, tectonic erosion, crustal uplift, free-air gravity anomaly, plate interfaces, elastic dislocation theory.

1. Introduction

Free-air gravity anomaly in plate subduction zones is generally characterized by island-arc high, trench low, and outer-rise gentle high. In northeast Japan we can observe that the island-arc high of free-air gravity anomaly takes its maximum about the eastern coastline (TOMODA and FUJIMOTO, 1982; SANDWELL and SMITH, 1997). The free-air gravity anomaly reflects the cumulative effects of long-term crustal uplift and subsidence (surface mass excess and deficit) due to steady plate subduction (MATSU'URA and SATO, 1989; SATO and MATSU'URA, 1988, 1992, 1993). However, in northeastern Japan, we can observe the

[1] Department of Earth and Planetary Science, The University of Tokyo, 7-3-1 Hongo, Bunkyo-ku, Tokyo 113-0033, Japan. E-mail: hashi@eps.s.u-tokyo.ac.jp

[2] Department of Earth Sciences, Faculty of Science, Chiba University, 1-33 Yayoi-cho, Inage-ku, Chiba-shi, Chiba 263-8522, Japan.

significant discrepancy in spatial patterns between free-air gravity anomaly and current vertical crustal motion. Form fluvial-terrace heights, for example, TAJIKARA (2004) has estimated the average crustal uplift rates over northeast Japan arc to be 0.2–0.3 mm/yr for the last 0.12 million years (the late Quaternary period). From marine-terrace heights KOIKE and MACHIDA (2001) have reported the very slow crustal uplift along eastern coastlines in northeast Japan during the last 0.12 million years. From DSDP drilling and seismic reflection records von Huene and his coworkers (VON HUENE *et al.*, 1982; VON HUENE and LALLEMAND, 1990; VON HUENE and SCHOLL, 1991) have revealed steep subsidence in a broad region along the landward slope of the Japan trench. On the basis of these geological and geomorphological data we may conclude that the current crustal motion in northeast Japan is characterized by gentle uplift in the land area and steep subsidence in the sea area, with the neutral point near the eastern coastline.

In order to explain the steep subsidence in a broad region along the landward slope of the Japan trench, VON HUENE and LALLEMAND (1990) proposed a model of tectonic erosion that consists of frontal and basal erosion of the overriding plate. The frontal erosion removes rock and sediment masses at the front of the landward trench slope. The basal erosion removes rock masses on the underside of the overriding plate. Both frontal and basal erosion thin the wedge portion of the overriding plate and cause the subsidence of the landward slope of the trench. From the tectonic point of view the basal erosion has more essential meaning than the frontal erosion, because it causes landward retreat of the plate interface. In northeast Japan the landward retreat rate of the plate interface has been estimated to be 2–3 km/Myr (VON HUENE and LALLEMAND, 1990). Recently, HEKI (2004) proposed a mechanical model of basal erosion to simulate crustal deformation in northeast Japan. In his model the process of removing a certain amount of mass on the underside of the overriding plate is represented by the negative crack opening (crack closing) at the plate interface. However, the negative crack opening cannot satisfy the mass conservation of the subduction zone system unless some mechanism of mass transfer to the depths is assumed.

In the present study we propose another mechanical model of basal erosion and carry out 3-D simulation of steady plate subduction with tectonic erosion. In Section 2 we show a basic idea for modelling basal erosion, and construct the mechanical model. In Section 3 we examine the effect of tectonic erosion on vertical crustal motion through numerical simulation. In Section 4 we compute vertical crustal motion in northeast Japan with a realistic 3-D model of plate interface geometry, and demonstrate that the pattern of current vertical crustal motion in northeast Japan can be rationally explained by the steady plate subduction with tectonic erosion.

2. 3-D Modelling of Steady Plate Subduction with Tectonic Erosion

2.1. Representation of Mechanical Interaction at Plate Interfaces

In subduction zones oceanic plates descend beneath overriding plates at constant rates on a long-term average. The occurrence of large interplate earthquakes can be regarded as

the perturbation of steady plate subduction. Thus, we may express crustal deformation in subduction zones as the superposition of the secular change due to steady slip over the whole plate interface and the cyclic change due to stick-slip motion in seismogenic regions. The steady slip motion along a plate interface brings about long-term vertical crustal deformation, characterized by island-arc uplift and trench subsidence (MATSU'URA and SATO, 1989; SATO and MATSU'URA, 1988, 1992, 1993). The stick-slip motion brings about cyclic crustal deformation around the seismogenic regions (HASHIMOTO and MATSU'URA, 2000, 2002).

Mechanical interaction at a plate interface is rationally represented by the increase of tangential displacement discontinuity across it (MATSU'URA and SATO, 1989). In general, the tangential displacement discontinuity (fault slip) is mathematically equivalent to the force system of a double-couple without moment (MARUYAMA, 1963; BURRIGE and KNOPOFF, 1964), which has no net force and no net torque. Such a property must be satisfied for any force system acting on plate interfaces, since it originates from dynamic processes within the Earth. Thus, given relative plate motion vectors, we can quantitatively describe the crustal deformation processes caused by plate subduction on the basis of elastic/viscoelastic dislocation theory.

2.2. *Long-term Crustal Deformation due to Steady Plate Subduction*

We model the lithosphere-asthenosphere system by a two-layered Maxwellian viscoelastic half-space. The constitutive equations of the surface layer and the underlying half-space are given by

$$\dot{\sigma}_{ij} + \frac{\mu^{(l)}}{\eta^{(l)}}\left(\sigma_{ij} - \frac{1}{3}\sigma_{kk}\delta_{ij}\right) = \lambda^{(l)}\dot{\varepsilon}_{kk}\delta_{ij} + 2\mu^{(l)}\dot{\varepsilon}_{ij}. \tag{1}$$

Here, σ_{ij}, ε_{ij}, and δ_{ij} are the stress tensor, the strain tensor, and the unit diagonal tensor, respectively, $\lambda^{(l)}$ and $\mu^{(l)}$ ($l = 1, 2$) are the Lamé elastic constants, and $\eta^{(l)}$ ($l = 1, 2$) denotes the viscosity of each medium. The dot indicates differentiation with respect to time. It should be noted that the viscosity of the lithosphere (the surface layer) is considerably larger than that of the asthenosphere (the underlying half-space). The standard values of structural parameters used for computation are listed in Table 1.

We introduce a 3-D curved interface Σ that divides the surface layer into two plates. In general, according to BACKUS and MULCAHY (1976), the surface moment tensor density corresponding to a tangential displacement discontinuity (fault slip) vector $\boldsymbol{u}^{(s)}$ at a point $\boldsymbol{\xi}$ on an interface Σ can be represented as

$$m_{pq}(\boldsymbol{\xi}) = \mu\, u^{(s)}(\boldsymbol{\xi})\, \left[\chi_p(\boldsymbol{\xi})n_q(\boldsymbol{\xi}) + \chi_q(\boldsymbol{\xi})n_p(\boldsymbol{\xi})\right], \tag{2}$$

where μ is the rigidity of the medium, $\boldsymbol{n}$ is the unit normal vector of Σ, $u^{(s)}$ is the magnitude of $\boldsymbol{u}^{(s)}$, and $\boldsymbol{\chi}$ is the unit slip-direction vector satisfying the orthogonality condition $\boldsymbol{n} \cdot \boldsymbol{\chi} = 0$. Then, the i-component of viscoelastic displacement (slip-response

Table 1

Structural parameters used in numerical simulations

	h [km]	ρ [kg/m^3]	λ [GPa]	μ [GPa]	η [Pa s]
Lithosphere	40	3000	40	40	5×10^{23}
Asthenosphere	∞	3400	90	60	5×10^{18}

h: thickness, ρ: density, λ and μ: Lamé elastic constants, η: viscosity.

function) $U_i(i = x, y, z)$ at a point $\boldsymbol{x}$ and time t due to a unit step slip at a point $\boldsymbol{\xi}$ and time τ is given by

$$U_i(\boldsymbol{x}, t; \boldsymbol{\xi}, \tau) = \mu F_{ipq}(\boldsymbol{x}, t; \boldsymbol{\xi}, \tau) [\chi_p(\boldsymbol{\xi}) n_q(\boldsymbol{\xi}) + \chi_q(\boldsymbol{\xi}) n_p(\boldsymbol{\xi})]. \tag{3}$$

Here, the function $F_{ipq}(\boldsymbol{x}, t; \boldsymbol{\xi}, \tau)$ denotes the i-component of viscoelastic displacement due to the pq-element of the moment tensor density with the magnitude $u^{(s)} = 1$. Then, we can compute the displacement field $u_i(i = x, y, z)$ due to arbitrary fault slip distribution $w(\boldsymbol{\xi}, \tau)$ on the plate interface Σ by using the technique of hereditary integral as

$$u_i(\boldsymbol{x}, t) = \int_{-\infty}^{t} \int_{\Sigma} U_i(\boldsymbol{x}, t - \tau; \boldsymbol{\xi}, 0) \frac{\partial w(\boldsymbol{\xi}, \tau)}{\partial \tau} d\boldsymbol{\xi} d\tau. \tag{4}$$

In the present problem we focus on vertical surface displacements u_z. For example, MATSU'URA and SATO (1989) and SATO and MATSU'URA (1993) give the explicit expressions of the viscoelastic slip-response function U_z for a viscoelastic multi-layered half-space under gravity.

Now we decompose the total fault slip motion w into the steady slip at a plate convergence rate v_{pl} and its perturbation Δw (forward slip due to interplate earthquakes and slip deficit due to interplate coupling) as

$$w(\boldsymbol{\xi}, \tau) = v_{pl}(\boldsymbol{\xi})\, \tau + \Delta w(\boldsymbol{\xi}, \tau). \tag{5}$$

Substituting this expression into Eq. (4), we obtain

$$u_z(\boldsymbol{x}, t) = \int_{t_0}^{t} \int_{\Sigma} U_z(\boldsymbol{x}, t - \tau; \boldsymbol{\xi}, 0) v_{pl}(\boldsymbol{\xi})\, d\boldsymbol{\xi} d\tau + \int_{t_0}^{t} \int_{\Sigma} U_z(\boldsymbol{x}, t - \tau; \boldsymbol{\xi}, 0) \frac{\partial \Delta w(\boldsymbol{\xi}, \tau)}{\partial \tau}\, d\boldsymbol{\xi} d\tau. \tag{6}$$

Here, we supposed that the fault slip motion (plate subduction) started at a time $t = t_0$. The first and the second terms on the right-hand side of Eq. (6) indicate the contributions from the steady slip motion and its perturbation, respectively. In the present problem where we are interested in long-term crustal deformation, we can neglect the second term, because it does not bring about secular changes. Thus the crustal uplift rate at a point $\boldsymbol{x}$ due to steady plate subduction after $t = t_0$ is given by

$$\dot{u}_z(\boldsymbol{x},t) = V_\Sigma(\boldsymbol{x},t-t_0) \equiv \int_\Sigma U_z(\boldsymbol{x},t-t_0;\boldsymbol{\xi},0)\, v_{pl}(\boldsymbol{\xi})\, d\boldsymbol{\xi}, \tag{7}$$

where the dot indicates differentiation with respect to time t, and $V_\Sigma(\boldsymbol{x},t)$ is the abbreviated representation of the integral of the slip-response function $U_z(\boldsymbol{x},t;\boldsymbol{\xi},0)$ over the plate interface Σ.

As shown in Table 1, the lithosphere-asthenosphere system consists of a high-viscosity surface-layer and a low-viscosity underlying half-space. Therefore, the viscoelastic vertical crustal deformation u_z has three different phases; instantaneous deformation of the elastic layered half-space, intermediate-term deformation of the elastic surface layer floating on the completely relaxed asthenosphere, and long-term deformation of the viscoelastic layered half-space after the completion of stress relaxation both in the asthenosphere and the lithosphere. Assuming the viscosity of the asthenosphere and the lithosphere to be $10^{18} - 10^{19}$ Pa s and $10^{23} - 10^{24}$ Pa s, respectively, the effective stress-relaxation times of the asthenosphere T_A and the lithosphere T_L become $10 - 10^2$ yr and $10^6 - 10^7$ yr, respectively (SATO and MATSU'URA, 1993). Then, we consider two representative cases; the case of young subduction zones, where the duration $t - t_0$ of steady plate subduction is much longer than T_A but much shorter than T_L, and the case of old subduction zones, in which the duration of steady plate subduction is much longer than T_L.

2.2.1. Young subduction zones. In the first case, $T_A << t - t_0 << T_L$, the asthenosphere has completely relaxed, although the lithosphere still behaves like an elastic plate. Then the slip response function U_z can be regarded as constant in time on this time scale. Denoting the slip response function on this time scale by $U_z^{(E)}(\boldsymbol{x};\boldsymbol{\xi})$, we can rewrite Eq. (7) as

$$\dot{u}_z(\boldsymbol{x},t) = V_\Sigma^{(E)}(\boldsymbol{x}) \equiv \int_\Sigma U_z^{(E)}(\boldsymbol{x};\boldsymbol{\xi}) v_{pl}(\boldsymbol{\xi}) d\boldsymbol{\xi} \quad \text{for} \quad T_A << t - t_0 << T_L. \tag{8}$$

The above equation means that the amount of crustal uplift increases with time at constant rates in young subduction zones.

2.2.2. Old subduction zones. In the second case, $t - t_0 >> T_L$, not only the asthenosphere but also the lithosphere has completely relaxed. In this case, since the slip response function U_z becomes zero, we can rewrite Eq. (7) as

$$\dot{u}_z(\boldsymbol{x},t) = 0 \quad \text{for} \quad t - t_0 >> T_L. \tag{9}$$

The above equation means that the amount of crustal uplift no longer increases in old subduction zones.

2.3. *Effects of Tectonic Erosion*

Now, we consider the effect of tectonic erosion in plate subduction zones. The physicochemical process of tectonic erosion may be very complex. However, from a mechanical point of view, we can regard this process as a mass transfer process from the underside of the overriding plate to the depths. Such a mass transfer process inevitably accompanies a landward retreat of the interface between the descending and the overriding plates. The progress of tectonic erosion would also produce changes in plate interface geometry. In the present study, however, we simply assume that the plate interface migrates landward at a constant rate v_e in the direction of plate convergence $(\cos\theta,\ \sin\theta,\ 0)$ without change in its geometry. Then, assuming that tectonic erosion started at $t = t_i$ in a part Σ' of the plate interface Σ, we can incorporate the effect of tectonic erosion into the first term on the right-hand side of Eq. (6) (the second term has been neglected) by replacing the argument $\boldsymbol{\xi}$ with $\boldsymbol{\xi} + \boldsymbol{v_e}\,(t - t_i)$ for the migrating interface Σ' as

$$\begin{aligned} u_z(\boldsymbol{x}, t) = &\int_{t_0}^{t} \int_{\Sigma-\Sigma'} U_z(\boldsymbol{x}, t-\tau;\boldsymbol{\xi}, 0) v_{pl}(\boldsymbol{\xi})\, d\boldsymbol{\xi} d\tau \\ &+ \int_{t_0}^{t_i} \int_{\Sigma'} U_z(\boldsymbol{x}, t-\tau;\boldsymbol{\xi}, 0) v_{pl}(\boldsymbol{\xi})\, d\boldsymbol{\xi} d\tau \\ &+ \int_{t_i}^{t} \int_{\Sigma'} U_z(\boldsymbol{x}, t-\tau;\boldsymbol{\xi} + \boldsymbol{v_e}\,(t-t_i), 0) v_{pl}(\boldsymbol{\xi} + \boldsymbol{v_e}\,(t-t_i))\, d\boldsymbol{\xi} d\tau \end{aligned} \tag{10}$$

Here, $\boldsymbol{v_e} = (v_e \cos\theta,\ v_e \sin\theta,\ 0)^T$ is the landward-retreat rate vector of the plate interface Σ', and the superscript T denotes the transpose of the corresponding vector.

Using the approximation of $v_{pl}(\boldsymbol{\xi} + \boldsymbol{v_e}\,(t - t_i)) \cong v_{pl}(\boldsymbol{\xi})$ and a symmetric property of $U_z(\boldsymbol{x}, t-\tau;\boldsymbol{\xi} + \boldsymbol{v_e}\,(t-t_i), 0) = U_z(\boldsymbol{x} - \boldsymbol{v_e}\,(t-t_i), t-\tau;\boldsymbol{\xi}, 0)$, we can rewrite Eq. (10) as

$$u_z(\boldsymbol{x}, t) = \int_{t_0}^{t} V_{\Sigma-\Sigma'}(\boldsymbol{x}, t-\tau)\, d\tau + \int_{t_0}^{t_i} V_{\Sigma'}(\boldsymbol{x}, t-\tau) d\tau + \int_{t_i}^{t} V_{\Sigma'}(\boldsymbol{x} - \boldsymbol{v_e}(t-t_i), t-\tau)\, d\tau \tag{11}$$

with

$$V_{\Sigma}(\boldsymbol{x}, t-\tau) = \int_{\Sigma} U_z(\boldsymbol{x}, t-\tau;\boldsymbol{\xi}, 0) v_{pl}(\boldsymbol{\xi})\, d\boldsymbol{\xi}. \tag{12}$$

Differentiating both sides of Eq. (11) with respect to time t, we can obtain the expressions of crustal uplift rates due to steady plate subduction with tectonic erosion as follows. The differentiation of the first, second, and third terms on the right hand side of Eq. (11) with respect to time t yields, respectively,

$$\frac{d}{dt}\int_{t_0}^{t} V_{\Sigma-\Sigma'}(\boldsymbol{x}, t-\tau)d\tau = V_{\Sigma}(\boldsymbol{x}, t-t_0) - V_{\Sigma'}(\boldsymbol{x}, t-t_0), \tag{13}$$

$$\frac{d}{dt}\int_{t_0}^{t_i} V_{\Sigma'}(\boldsymbol{x}, t-\tau)d\tau = -V_{\Sigma'}(\boldsymbol{x}, t-t_i) + V_{\Sigma'}(\boldsymbol{x}, t-t_0), \tag{14}$$

and

$$\begin{aligned}\frac{d}{dt}\int_{t_i}^{t} V_{\Sigma'}(\boldsymbol{x}-\boldsymbol{v_e}\,(t-t_i), t-\tau) &= V_{\Sigma'}(\boldsymbol{x}, t-t_i)\\ &- v_e\cos\theta\int_{t_i}^{t} V_{\Sigma',x}(\boldsymbol{x}-\boldsymbol{v_e}\,(t-t_i), t-\tau)\,d\tau\\ &- v_e\sin\theta\int_{t_i}^{t} V_{\Sigma',y}(\boldsymbol{x}-\boldsymbol{v_e}\,(t-t_i), t-\tau)\,d\tau\end{aligned} \tag{15}$$

with

$$V_{,x(y)}(\boldsymbol{x}, t-\tau) = \frac{\partial}{\partial x(y)} V(\boldsymbol{x}, t-\tau). \tag{16}$$

Thus the crustal uplift rates due to steady plate subduction with tectonic erosion are given by

$$\dot{u}_z(\boldsymbol{x}, t) = V_{\Sigma}(\boldsymbol{x}, t-t_0) - \int_{t_i}^{t} \boldsymbol{v}_e \cdot \nabla V_{\Sigma'}(\boldsymbol{x}-\boldsymbol{v_e}(t-t_i), t-\tau)\,d\tau. \tag{17}$$

Here, the first term on the right-hand side of the above equation represents the effects of steady slip motion over the whole plate interface Σ, which is the same as that in Eq. (7), and the second term represents the effects of the landward retreat of the plate interface Σ' due to tectonic erosion. When the migration distance of the plate interface Σ' during $t - t_i$ is much smaller than the horizontal distance between the migrating plate interface and observation points, that is, $|\boldsymbol{v}_e\,(t-t_i)| << |\boldsymbol{x}-\boldsymbol{\xi}|$, we can obtain the following approximate expression of Eq. (17):

$$\dot{u}_z(\boldsymbol{x}, t) \cong V_{\Sigma}(\boldsymbol{x}, t-t_0) - \int_{t_i}^{t} \boldsymbol{v}_e \cdot \nabla V_{\Sigma'}(\boldsymbol{x}, t-\tau)\,d\tau \quad \text{for} \quad |\boldsymbol{v}_e\,(t-t_i)| << |\boldsymbol{x}-\boldsymbol{\xi}|. \tag{18}$$

Now we consider three representative cases: 1) Young subduction zones, in which the duration of both tectonic erosion $t - t_i$ and steady plate subduction $t - t_0$ are

much longer than the effective stress-relaxation time of the asthenosphere T_A but much shorter than the effective stress-relaxation time of the lithosphere T_L, 2) moderate-aged subduction zones, in which the duration of tectonic erosion is by much longer than T_A but much shorter than T_L, and that of steady plate subduction is much longer than T_L, and 3) old subduction zones, in which the duration of both tectonic erosion and steady plate subduction are much longer than T_L.

2.3.1. Young subduction zones. In the first case, $T_A << t - t_i << T_L$ and $T_A << t - t_0 << T_L$, the integral of the slip-response function over the plate interface $V_\Sigma(\boldsymbol{x},t - t_0)$ and its spatial derivative $\nabla V_{\Sigma'}(\boldsymbol{x}, t - \tau)$ in of Eq. (18) can be regarded as constant in time. Denoting the slip response function on this time scale by $U_z^{(E)}(\boldsymbol{x};\boldsymbol{\xi})$, and its surface integral over Σ by $V_\Sigma^{(E)}(\boldsymbol{x}) \equiv \int_\Sigma U_z^{(E)}(\boldsymbol{x};\boldsymbol{\xi}) v_{pl}(\boldsymbol{\xi}) d\boldsymbol{\xi}$, we can obtain the expression of crustal uplift rates in the case of young subduction zones ($T_A << t - t_i << T_L$ and $T_A << t - t_0 << T_L$) as

$$\dot{u}_z(\boldsymbol{x}, t) = V_\Sigma^{(E)}(\boldsymbol{x}) - \boldsymbol{v}_e \cdot \nabla V_{\Sigma'}^{(E)}(\boldsymbol{x})\ (t - t_i). \tag{19}$$

The above equation means that both effects of tectonic erosion on Σ' and steady plate subduction over Σ contribute to crustal uplift and subsidence in young subduction zones.

2.3.2. Moderate-aged subduction zones. In the second case, $T_A << t - t_i << T_L$ and $t - t_0 >> T_L$, the integral of the slip-response function over the plate interface $V_\Sigma(\boldsymbol{x},t - t_0)$ becomes zero, however its spatial derivative $\nabla V_{\Sigma'}(\boldsymbol{x}, t - \tau)$ takes the same constant value as in the first case. Then, we can obtain the expression of crustal uplift rates in the case of moderate-aged subduction zones ($T_A << t - t_i << T_L$ and $t - t_0 >> T_L$) as

$$\dot{u}_z(\boldsymbol{x}, t) = -\boldsymbol{v}_e \cdot \nabla V_{\Sigma'}^{(E)}(\boldsymbol{x})\ (t - t_i)\,. \tag{20}$$

The above equation means that only the effect of tectonic erosion contributes to crustal uplift and subsidence in moderate-aged subduction zones.

2.3.3. Old subduction zones. In the third case, $t - t_i >> T_L$ and $t - t_0 >> T_L$, both the integral of the slip-response function over the plate interface $V_\Sigma(\boldsymbol{x},t - t_0)$ and its spatial derivative $\nabla V_{\Sigma'}(\boldsymbol{x}, t - \tau)$ become zero. Then, in the case of old subduction zones ($t - t_i >> T_L$ and $t - t_0 >> T_L$), we obtain

$$\dot{u}_z(\boldsymbol{x}, t) = 0. \tag{21}$$

The above equation means that even tectonic erosion no longer brings about to crustal uplift and subsidence in old subduction zones.

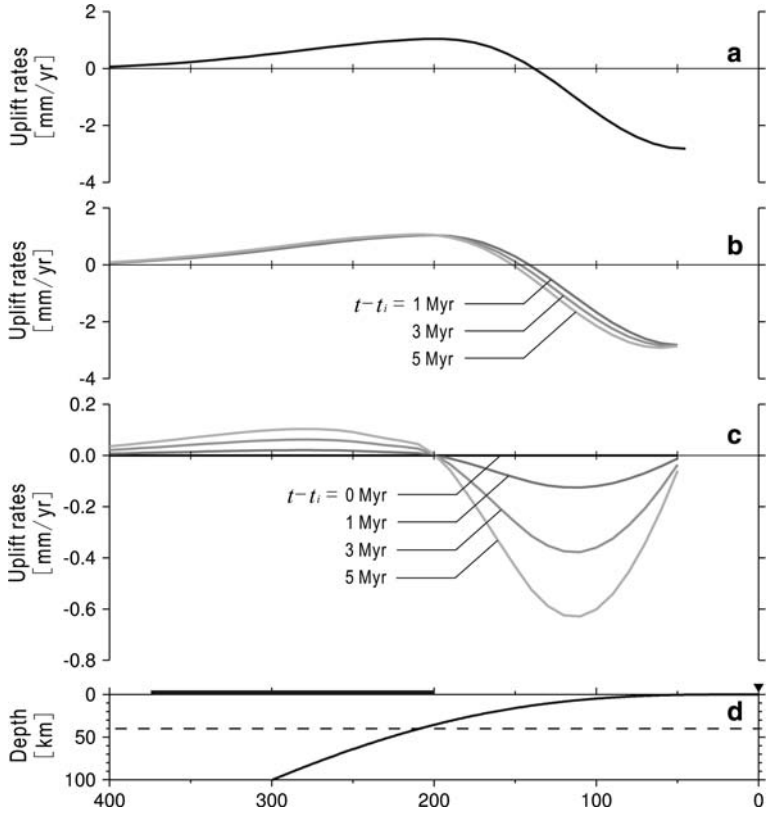

Figure 1

Computed vertical crustal motion due to steady plate subduction with tectonic erosion. (a) The surface uplift rates due to steady plate subduction. (b) The temporal change in surface uplift rates in young subduction zones with tectonic erosion. The uplift rates are given by the sum of the surface uplift rates due to steady plate subduction (a) and tectonic erosion (c). (c) The surface uplift rates due to tectonic erosion after the duration $t - t_i = 0$, 1, 3, and 5 Myr. The landward retreat rate of the plate interface is taken to be 3 mm/yr. (d) The trench-across vertical section of the plate interface. The thick horizontal line indicates the range of the land area in northeast Japan. The solid triangle indicates the position of the trench axis. The dotted line indicates the lithosphere-asthenosphere boundary.

3. Vertical Crustal Motion Caused by Tectonic Erosion

The vertical crustal motion due to steady plate subduction with tectonic erosion can be expressed in the form of Eq. (17). In this section, in order to quantitatively examine the effect of tectonic erosion, we carry out numerical simulation with simplified plate interface geometry.

We consider an infinitely long plate interface Σ along the trench axis. The trench-across vertical section of the plate interface is shown in Figure 1d. We take the rate of fault slip along the plate interface to be 8 cm/yr with its direction perpendicular to the trench axis. Furthermore, we suppose that the whole plate interface migrates landward at a constant rate

of 3 mm/yr. Consequently, we can treat the problem in a 2-D framework. Taking the y axis so as to coincide with the trench axis, the x axis on the surface to be perpendicular to the trench axis, and the z axis to be vertical upward, we can rewrite Eq. (17) as

$$\dot{u}_z(\boldsymbol{x}, t) = V_\Sigma(\boldsymbol{x}, t - t_0) - v_e \int_{t_i}^{t} \frac{\partial}{\partial x} V_\Sigma(\boldsymbol{x} - \boldsymbol{v_e}(t - t_i), t - \tau)\, d\tau. \tag{22}$$

Here, the first and second terms on the right-hand side of the above equation represent the effects of steady plate subduction and landward retreat of the plate interface due to tectonic erosion, respectively. On a time-scale where the lithosphere can be regarded as an elastic surface layer floating on the completely relaxed asthenosphere, Eq. (22) can be rewritten in the form of Eq. (19) as

$$\dot{u}_z(\boldsymbol{x}, t) = V_\Sigma^{(E)}(\boldsymbol{x}) - v_e(t - t_i) \frac{\partial}{\partial x} V_\Sigma^{(E)}(\boldsymbol{x}). \tag{23}$$

From the above equation we can see that the crustal uplift rate due to tectonic erosion (the second term) is given by the product of the migration distance $v_e\,(t - t_i)$ and the negative gradient of the crustal uplift rate due to steady plate subduction $\partial V_\Sigma^{(E)}(\boldsymbol{x})/\partial x$.

In Figure 1a we show the computed crustal uplift rates due to steady plate subduction, characterized by island-arc high and trench low. In Figure 1c we show the computed crustal uplift rates due to tectonic erosion ($v_e = 3$ mm/yr) for the duration $t - t_i = 0$, 1, 3, and 5 Myr. From this figure we can see that tectonic erosion brings about the steep subsidence of the wedge portion of the overriding plate and the gentle uplift of the landward portion. The zero crossing point of the uplift rate curves agrees with the point of the maximum crustal uplift rate due to steady plate subduction. Figure 1b shows the temporal change of crustal uplift rates in young subduction zones with tectonic erosion ($T_A << t - t_i << T_L$ and $T_A << t - t_0 << T_L$), which is given by the sum of the crustal uplift rates due to steady plate subduction (Fig. 1a) and tectonic erosion (Fig. 1c). Here, it should be noted that Eq. (23) is not applicable for the points near the migrating plate interface, because the approximate expression in Eq. (18) is not valid there. From Figure 1b we can see that the effect of tectonic erosion is less significant in young subduction zones. However, in old subduction zones ($T_A << t - t_i << T_L$ and $t - t_0 >> T_L$), the effect of tectonic erosion becomes dominant, because the crustal uplift rates due to steady plate subduction (the first term of Eq. (22)) tend to zero. In other words, the initiation of tectonic erosion in old subduction zones causes significant change in the mode of vertical crustal motion.

4. Vertical Crustal Motion in Northeast Japan

4.1. 3-D Plate Interface Geometry in and Around Japan

Recently, HASHIMOTO *et al.* (2004) constructed a realistic 3-D model of plate interface geometry in and around Japan on the basis of the topography of ocean floors

and the hypocenter distribution of earthquakes (Fig. 2). The modelled region extends from 125°E to 155°E in longitude and from 20°N to 50°N in latitude (about 3000 km $\times$ 3000 km). In this region the lithosphere is divided into four plates; the Pacific (PA), North American (NA), Philippine Sea (PH), and Eurasian (EU) plates. Since the interface between the North American plate and the Eurasian plate is indefinite, we discard it in modelling. The 3-D geometry of the upper boundaries of the Pacific and Philippine Sea plates is represented by the superposition of bi-cubic B-splines with 8 km equally spaced local supports. The expansion coefficients of plate interface geometry are determined from ISC (International Seismological Centre) hypocenter location data by using an inversion technique developed by YABUKI and MATSU'URA (1992).

In order to determine the direction of steady slip vectors $\boldsymbol{v}_{pl}$ on the four given plate interfaces, Σ_1 (PA-NA), Σ_2 (PA-PH), Σ_3 (PH-NA) and Σ_4 (PH-EU), first, we calculate the relative plate motion vector $\boldsymbol{v} = (v_x, v_y, 0)^T$ at each plate boundary from NUVEL-1A (DEMETS *et al*., 1994) as shown in Figure 3. Then, we project the calculated relative plate motion vector $\boldsymbol{v}$ onto the plate interface. The depth to the plate interface is defined by the

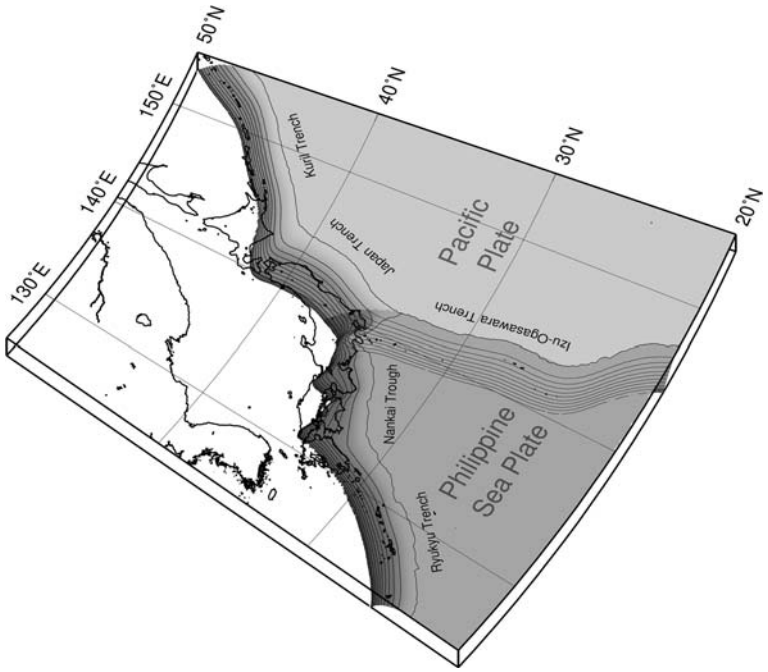

Figure 2

A 3-D model of plate interface geometry in and around Japan, used in numerical simulations. The upper boundaries of the descending Pacific and the Philippine Sea plates are shown. The intervals of the isodepth contours are taken to be 10 km. The model region extends from 125°E to 155°E in longitude and from 20°N to 50°N in latitude.

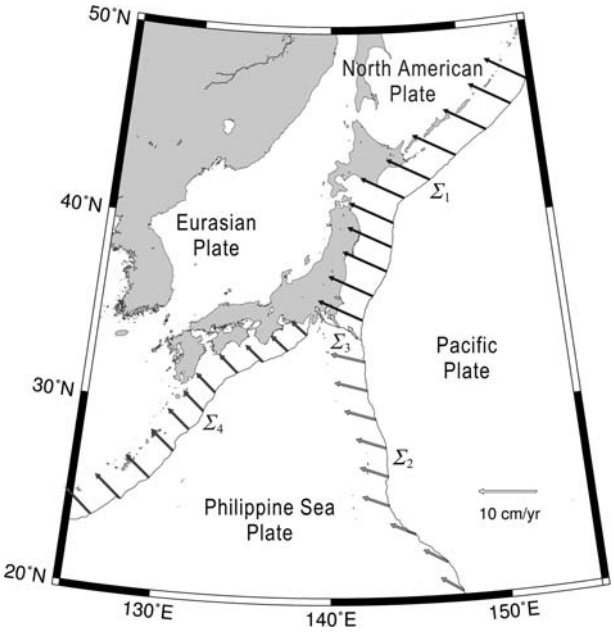

Figure 3
Plate boundaries and relative plate motion vectors in and around Japan. The elastic lithosphere is divided into four plates; the Pacific (PA), the North American (NA), the Philippine Sea (PH), and the Eurasian (EU) plates. These four plates are interacting with each other at four plate interfaces; Σ_1 (PA-NA), Σ_2 (PA-PH), Σ_3 (PH-NA) and Σ_4 (PH-EU). The relative plate motion vectors (thick arrows) are calculated from the global plate motion model NUVEL-1A (DeMets *et al.*, 1994).

continuous function $z = z(x, y)$, and therefore the unit normal vector $\boldsymbol{n}$ of the plate interface is given by

$$\boldsymbol{n} = \begin{pmatrix} n_x \\ n_y \\ n_z \end{pmatrix} = \frac{1}{\sqrt{(\partial z/\partial x)^2 + (\partial z/\partial y)^2 + 1}} \begin{pmatrix} -\partial z/\partial x \\ -\partial z/\partial y \\ 1 \end{pmatrix}. \tag{24}$$

The magnitude v_{pl} of the steady slip vector at the plate interface is taken to be the same as the magnitude of the relative plate motion vector $\boldsymbol{v}$ to satisfy the mass conservation of the descending slab. Then, the steady slip vector $\boldsymbol{v}_{pl}$ is given by

$$\boldsymbol{v}_{pl} = |\boldsymbol{v}|\,\boldsymbol{\chi} = \frac{\sqrt{v_x^2 + v_y^2}}{\sqrt{v_x^2 + v_y^2 + \left(v_x n_x + v_y n_y\right)^2 / n_z^2}} \begin{pmatrix} -v_x \\ -v_y \\ \left(v_x n_x + v_y n_y\right)/n_z \end{pmatrix}. \tag{25}$$

Here, $\boldsymbol{\chi}$ represents the unit slip-direction vector, which is parallel to the projection of the relative plate motion vector $\boldsymbol{v}$ onto the plate interface.

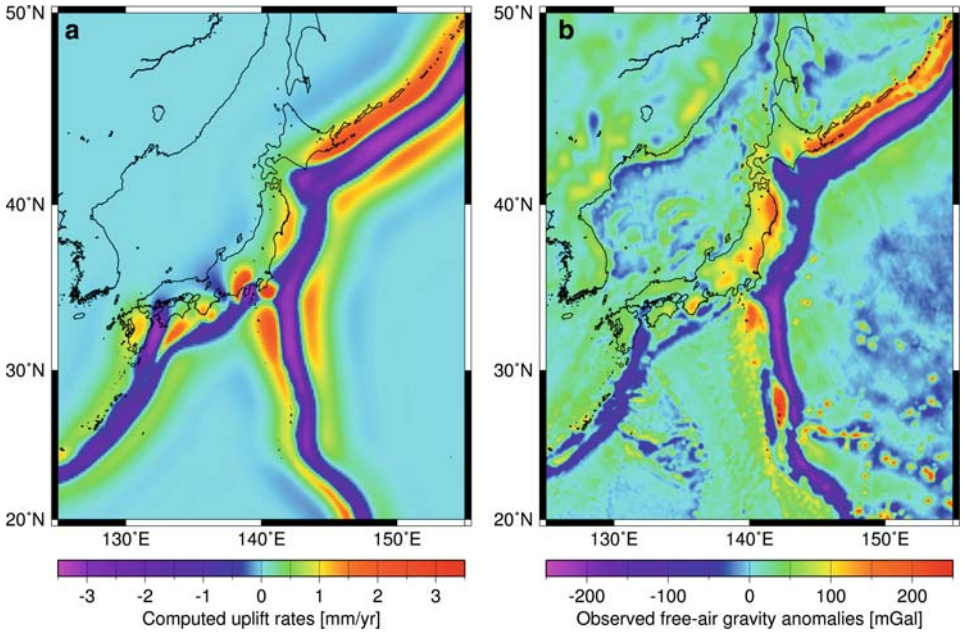

Figure 4

Computed surface uplift rates and observed free-air gravity anomalies in and around Japan. (a) The surface uplift rates due to simple steady subduction of the Pacific and the Philippine Sea plates. The maximum subsidence rates at the Japan trench and the Nankai through are about 2.5 mm/yr and 1.5 mm/yr, respectively. The maximum uplift rate is approximately 1.5 mm/yr, both in northeast Japan and southwest Japan. (b) Free-air gravity anomalies obtained by satellite altimetry (SANDWELL and SMITH, 1997). The color bar shows the amplitude of free-air gravity anomaly.

4.2. Vertical Crustal Motion in Northeast Japan

First, we compute long-term crustal motion in northeast Japan due to steady plate subduction without tectonic erosion. Carrying out the integration in Eq. (8) over all the plate interfaces $\Sigma = \Sigma_1 + \Sigma_2 + \Sigma_3 + \Sigma_4$, we obtain the surface uplift rates due to steady plate subduction. In Figure 4 we show the computed surface uplift rates together with the free-air gravity anomalies obtained by satellite altimetry (SANDWELL and SMITH, 1997). From comparison of the patterns of computed surface uplift rates (Fig. 4a) and observed free-air gravity anomalies (Fig. 4b), we can see that the 3-D model of simple steady plate subduction adequately reproduces not only the general pattern of free-air gravity anomaly (island-arc high, trench low and outer-rise gentle high) but also the regional patterns of negative anomaly at the Kuril-Japan trench junction in northeast Japan and the Nankai trough-Ryukyu trench junction in southwest Japan. This means that the essential cause of free-air gravity anomaly in and around Japan is in long-term crustal uplift and subsidence due to simple steady plate subduction. As mentioned in Subsection 2.2, Eq. (8) is an approximate expression in the case of young subduction zones; that is,

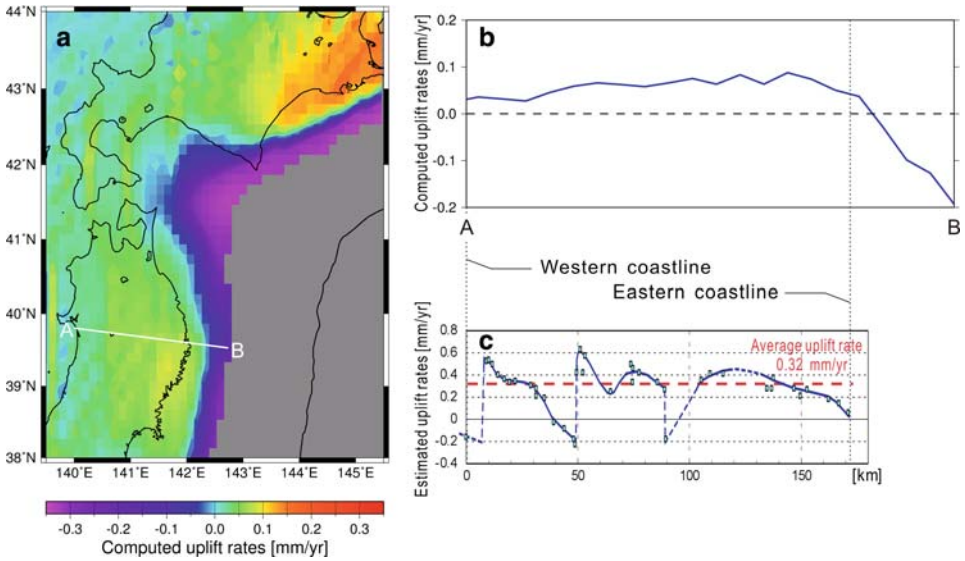

Figure 5

Computed and observed surface uplift rates in northeast Japan. (a) The pattern of computed surface uplift rates due to steady plate subduction with tectonic erosion. The landward-retreat rate and the duration of tectonic erosion are taken to be 3 mm/yr and 3.5 Myr, respectively. The color bar shows the amplitude of the computed surface uplift rates. (b) The profile of the computed surface uplift rates along the line A-B in Figure 5a. (c) The average crustal uplift rates during the last 0.12 million years, estimated from fluvial-terrace heights by TAJIKARA (2004). The average crustal uplift rate over the northeast Japan arc is about 0.3 mm/yr. The short-wavelength (10–50 km) deformation in the western part of the northeast Japan arc is ascribed to the thrust motion of active faults. The crustal uplift rate in the eastern part of the northeast Japan arc gradually decreases eastward to zero near the eastern coastline.

the duration of steady plate subduction is much shorter than the effective stress-relaxation time of the lithosphere. If the duration of steady plate subduction becomes longer, the surface uplift rates gradually decrease as a whole with time and finally tend to zero because of stress relaxation in the lithosphere (SATO and MATSU'URA, 1993). From the ages of islands and seamounts at the northwestern end of the Hawaiian Chain, the duration of the steady subduction of the Pacific plate beneath northeast Japan in the present direction is simply estimated about 40 Myr, which is much longer than the effective stress-relaxation time of the lithosphere. Thus, we can explain the stable pattern of free-air gravity anomaly by the simple steady plate subduction model, but not the pattern of current surface uplift rates observed in northeast Japan.

In northeast Japan, as shown in Figure 4b, the island-arc high of observed free-air gravity anomaly takes its maximum about the eastern coastline, while the current crustal motion estimated from geological and geomorphological observations shows gentle uplift in the land area and steep subsidence in the sea area with the neutral point near the eastern coastline. In order to explain this discrepancy, we compute long-term crustal uplift rates due to steady plate subduction with tectonic erosion. Now we consider the case of old

subduction zones ($T_A << t - t_i << T_L$ and $t - t_0 >> T_L$), and assume the landward migration of the Pacific-North American plate interface ($\Sigma' = \Sigma_1$) at a constant rate in the direction of relative plate motion (N63°W). From Eq. (20), carrying out the integration of the second term on the right-hand side in Eq. (18) over the migrating plate interface $\Sigma' = \Sigma_1$, we can obtain the surface uplift rates in northeast Japan due to steady plate subduction with tectonic erosion. The landward retreat rate v_e is taken to be 3 mm/yr on the basis of the geological estimate by VON HUENE and LALLEMAND (1990). According to SATO (1994), the mode of tectonic loading in northeast Japan has changed from extension to compression 3.5 million years ago. Then, we take the duration of tectonic erosion $t - t_i$ to be 3.5 Myr, which is considerably shorter than the effective stress-relaxation time of the lithosphere T_L. In Figure 5a we show the pattern of computed surface uplift rates in northeast Japan, characterized by gradual uplift over the northeast Japan arc and steep subsidence in the sea area with the neutral point near the eastern coastline. In Figures 5b and c we show the profile of the computed surface uplift rates along the line A-B (Fig. 5a) and that of the average crustal uplift rates during the last 0.12 million years estimated from fluvial-terrace heights by TAJIKARA (2004), respectively. From these figures we can see that the 3-D model of steady plate subduction with tectonic erosion adequately reproduces the pattern of current vertical crustal motion in northeast Japan.

The tectonic evolution model is based on the assumption that tectonic erosion at a constant rate has started 3–4 million years ago after the long duration of simple steady plate subduction. From Figures 5b and c we can find that the computed surface uplift rate is somewhat small in comparison with the observed crustal uplift rate. It should be noted that the observed crustal uplift rate includes not only the direct effect of tectonic erosion but also the indirect effect of crustal thickening. TAJIKARA (2004) suggested that his estimates of crustal uplift rates include the effect of crustal thickening of the northeast Japan arc by East-West compression. Actually, in northeast Japan, there exist many thrust faults and folds with their strikes parallel to North-South direction (e.g., RESEARCH GROUP FOR ACTIVE FAULTS OF JAPAN, 1991; SATO, 1994; TAJIKARA, 2004). The short-wavelength (10–50 km) deformation on the west side of the northeast Japan arc in Figure 5c can be ascribed to the thrust motion of such active faults (TAJIKARA, 2004).

5. Discussion and Conclusions

Free-air gravity anomaly in plate subduction zones reflects the cumulative effects of long-term crustal uplift and subsidence due to steady plate subduction. In northeast Japan, however, the island-arc high of free-air gravity anomaly takes its maximum about the eastern coastline, while the current vertical crustal motion shows gentle uplift in the land area and steep subsidence in the sea area with the neutral point near the eastern coastline. Such a discrepancy in spatial patterns between free-air gravity anomaly and current vertical crustal motion can be rationally explained by considering the effect of tectonic

erosion at the PA-NA plate interface, which started 3–4 Myr ago after the long duration of simple steady plate subduction.

We developed a mechanical model of steady plate subduction with tectonic erosion on the basis of elastic/viscoelastic dislocation theory. Through numerical simulations with this model we demonstrated that the pattern of free-air gravity anomaly in northeast Japan could be explained by simple steady slip at the PA-NA plate interface at the early stage of subduction. We also demonstrated that the pattern of current vertical crustal motion could be explained by steady slip with tectonic erosion at the late stage of subduction. From these simulation results we proposed a tectonic evolution model which can consistently explain both patterns of free-air gravity anomaly and current vertical crustal motion in northeast Japan.

The proposed tectonic evolution model is based on the assumption that tectonic erosion at a constant rate started 3–4 Myr ago after the long duration of simple steady plate subduction. At the late stage of subduction the surface uplift rate is proportional to the product of the tectonic erosion rate (the landward-retreat rate v_e of the plate interface) and the duration of tectonic erosion ($t - t_i$). In computation of the surface uplift rates in Figure 5b, which are significantly small in comparison with observed surface uplift rates, we took the landward-retreat rate and the duration of tectonic erosion to be 3 mm/yr and 3.5 Myr, respectively. As mentioned in subsection 2.4, the discrepancy between computed and observed uplift rates can be ascribed partly to the neglect of crustal-thickening effects and partly to the underestimate of the landward-retreat rate. If we ignore the effects of crustal thickening, we require the landward-retreat rate of about 12 mm/yr to account for the observed surface uplift rates. The surface uplift rates also increase with the duration of tectonic erosion, if it is much shorter than the effective stress-relaxation tine of the lithosphere T_L. In the present case, however, the duration of tectonic erosion (3.5 Myr) is of the same order as T_L (about 5 Myr), and thus we cannot expect the resolution of the discrepancy between computed and observed uplift rates by increasing the duration of tectonic erosion.

Acknowledgments

Computation of viscoelastic slip-response functions was performed on the Earth Simulator at the Earth Simulator Center, Japan Agency for Marine-Earth Science and Technology (JAMSTEC).

References

Backus, G. and Mulcahy, M. (1976), *Moment tensors and other phenomenological descriptions of seismic sources. II. Discontinuous displacements*, Geophys. J. R. astr. Soc. *46*, 301–329.

Burridge, R. and Knopoff, L. (1964), *Body force equivalents for seismic dislocations*, Bull. Seismol. Soc. Am. *54*, 1875–1888.

DeMets, C., Gordon, R. G., Argus, D. F., and Stein, S. (1994), *Effect of recent revisions to the geomagnetic reversal time scale on estimates of current plate motions*, Geophys. Res. Lett. *21*, 2191–2194.

Hashimoto, C. and Matsu'ura, M. (2000), *3-D physical modelling of stress accumulation and release processes at transcurrent plate boundaries*, Pure Appl. Geophys. *157*, 2125–2147.

Hashimoto, C. and Matsu'ura, M. (2002), *3-D simulation of earthquake generation cycles and evolution of fault constitutive properties*, Pure Appl. Geophys. *159*, 2175–2199.

Hashimoto, C., Fukui, K., and Matsu'ura, M. (2004), *3-D Modelling of plate interfaces and numerical simulation of long-term crustal deformation in and around Japan*, Pure Appl. Geophys. *161*, 2053–2067.

Heki, K. (2004), *Space geodetic observation of deep basal subduction erosion in northeastern Japan*. Earth Planet. Sci. Lett. *219*, 13–20.

Koike, K. and Machida, H., *Atlas of Quaternary marine terraces in the Japanese islands* (Univ. of Tokyo Press, Tokyo 2001).

Maruyama, T. (1963), *On the force equivalents of dynamical elastic dislocations with reference to the earthquake mechanism*, Bull. Earthq. Res. Inst., Tokyo Univ. *41*, 467–486.

Matsu'ura, M. and Sato, T. (1989), *A dislocation model for the earthquake cycle at convergent plate boundaries*, Geophys. J. Int. *96*, 23–32.

Research Group for Active Faults of Japan, *Active faults in and around Japan, sheet maps and inventories (revis. ed.)*, (Univ. of Tokyo Press, Tokyo 1991).

Sandwell, D. T. and Smith, W. H. F. (1997), *Marine gravity anomaly from Geosat and ERS 1 satellite altimetry*, J. Geophys. Res. *102*, 10039–10054.

Sato, H. (1994), *The relationship between late Cenozoic tectonic events and stress field and basin development in northeast Japan*, J. Geophys. Res. *99*, 22261–22274.

Sato, T. and Matsu'ura, M. (1988), *A kinematic model for deformation of the lithosphere at subduction zones*, J. Geophys. Res. *93*, 6410–6418.

Sato, T. and Matsu'ura, M. (1992), *Cyclic crustal movement, steady uplift of marine terraces, and evolution of the island arc-trench system in southwest Japan*, Geophys. J. Int. *111*, 617–629.

Sato, T. and Matsu'ura, M. (1993), *A kinematic model for evolution of island arc-trench systems*, Geophys. J. Int. *114*, 512–530.

Tajikara, M. (2004), *Vertical crustal movements of the northeast Japan arc in late Quaternary time*, Ph. D. Thesis, University of Tokyo.

Tomoda, Y. and Fujimoto, H. (1982), *Maps of gravity anomalies and bottom topography in Western Pacific*, Bull. Ocean Res. Int. Univ. Tokyo 14.

von Huene, R. and Lallemand, S. (1990), *Tectonic erosion along the Japan and Peru convergent margins*, Geol. Soc. Am. Bull. *102*, 704–720.

von Huene, R. and Scholl, D. W. (1991), *Observations at convergent margins concerning sediment subduction, subduction erosion, and the growth of continental crust*, Rev. Geophys. *29*, 279–316.

von Huene, R., Langseth, M., Nasu, N. and Okuda, H. (1982), *A summary of Cenozoic tectonic history along the IPOD Japan trench transect*, Geol. Soc. Am. Bull. *93*, 829–846.

Yabuki, T. and Matsu'ura, M. (1992), *Geodetic data inversion using a Bayesian information criterion for spatial distribution of fault slip*, Geophys. J. Int. *109*, 363–375.

(Received September 7, 2006, revised April 5, 2007, accepted May 30, 2007)
Published Online First: April 2, 2008